DIGITAL MOIRÉ APPLICATIONS TO REMOTE MEASURING TECHNIQUES

Roberto Torroba
Centro de Investigaciones Opticas (CIOp)
and
OPTIMO, Facultad de Ingeniería, Universidad Nacional de La
Plata, La Plata Argentina
e-mail: robertot@ciop.unlp.edu.ar

Abstract

A review of recent advances and applications in digital moiré is presented. Two particular cases are detailed, namely, the measurement of small rotation angles based on projection digital moiré and on self-imaging phenomenon, and an object positioning method using a model of moiré fringe visibility mismatching due to defocusing. In both cases a theoretical approach is described and experimental results are shown.

Resumen

Se presenta un análisis de los últimos avances y aplicaciones realizados con el uso de la técnica de moire digital. Se detallan dos casos en particular: la medición de pequeños ángulos de rotación basados en el more digital por proyección de franjas y en el fenómeno de las autoimagenes; y un método para el posicionado de objetos usando un modelo de compensación de visibilidades en las franjas de moire digital causado por desenfoques. En ambos casos se describe la teoría y se muestran los resultados experimentales que confirman la técnica propuesta.

INTRODUCTION

Holographic, speckle or moire fringe phenomena have been developed as applications in the metrology of surface form. These methods offer a wide range of sensitivities together with the ability to visualize the measurement parameter through a fringe pattern. At the beginning, the work in this field relied on subjective visual evaluation or laborious analysis of the fringe pattern. Interferometry can be used to produce a fringe pattern that represents the field surface alteration of an object due to some change. Digital speckle pattern interferometry (DSPI) is one of the most modern techniques for depicting such fringe patterns It combines real-time processing with the flexibility of software handling. DSPI was developed by combining the well-known techniques of holographic and speckle interferometry by using an image hologram setup and following the methods of double-exposure holography Digital processing removed much of this cumbersome analysis by offering the potential for rapid, automatic fringe interpretation. These techniques were prompted by advances in solid state detector arrays, processing technology and the development of powerful desk-top computers. The basic system consists of a CCD camera and equipment to store and compute analog or digitized images, where the results can be displayed on a monitor. In the following, we will restrict our attention to the moiré effect. In the classical moiré effect, fringe patterns are formed when two gratings are superimposed [1]. Metrological applications of this effect include strain analysis [2], vibration analysis [3] and contour mapping [4]. Among the different alternatives we have the projection based moiré technique, which involves projecting an equidistant grating, placed in front of the recording system. The recording step can be done in various ways, but electronic and digital processing are increasingly attractive, as explained above. Digitized moiré fringes were obtained in different ways, such as time averaging recording of vibrating surfaces, external video signals or electronic scanning and sampling techniques [5]. In any case, the difficulty of the analysis largely depends on the mathematics involved in describing the configuration of the moiré fringes. In general, there is no unified approach as to where and how the coordinate system are set.

In our case, Digital Moiré techniques are implemented by digital subtraction with the help of a CCD camera and an image processor. A given image of a grating, chosen as reference, is stored in the frame grabber of the image processor and subtracted at TV rate (30 frames per second) from the incoming one. The result is shown (in modulus) at a monitor. If the grating is rotated, the subtraction operation gives rise to a moiré pattern without needing of another grating. We can consider the situation as equivalent to the case of superposition with a virtual grating corresponding to the first stored reference image. In this approach, we consider the camera as a passive element that does not require any calibration. This technique offers clear advantages over traditional interferometric methods: there is no need to resolve high frequency (holographic type) fringes, no chemical development is required, no repositioning of photoplates, less stringent mechanical stability as in interferometric methods and the potential of software handling to the processing of image information. This last advantage induces a number of studies to investigate different alternatives of automatization, including FFT, filtering options, histograms, etc. According to the above discussion, digital moiré offers a promising and interesting alternative tool to the detection and evaluation in the non-destructive testing process.

In the present work we are concerned with two applications of measurement techniques by means of digital moire under different configurations, adapted to the measurement circumstances.

In the following sections, we will explain the practical techniques for each case: small angle measurement, focusing technique, and contouring with phase stepping. Experimental procedures, practical applications and theoretical explanations will be given in the next sections.

1. SMALL ANGLE MEASUREMENTS WITH DIGITAL MOIRÉ

We are here concerned with the tilt measurement of structures by means of digital moiré. Rather than a mathematical description, we adopt an approach which is based on the use of a

transfer curve, allowing a quick determination of the angle the structure rotated. The digital moiré technique is of the projection type, but instead of an imaging system for the projection, we make use of the Talbot or self-imaging phenomenon [6] to produce the grating image on the surface. In the following, we will explain the practical technique to obtain the fringes and the transfer curve. In connection with this approach, the errors of the system are estimated and experimental results are shown.

1.1.EXPERIMENTAL SET-UP AND PROCEDURE

The optical arrangement of this proposal is shown in Figure 1. This is a single beam projection type moiré configuration. Fringe projection can be accomplished in two ways, either by interference between mutually coherent waves or by imaging a grating. The working principle of the method is to project onto the object at oblique incidence a periodic pattern of bright and dark fringes (Ronchi ruling). As a main difference to previous techniques, we do not use any imaging system or projection device to image the grating onto the object, but we take advantage of the Talbot effect or self-imaging phenomenon. In this way, magnified replicas of the grating can be used with the advantage of tuning sensitivity. Besides, they are independent of the resolving power of any imaging projection system.

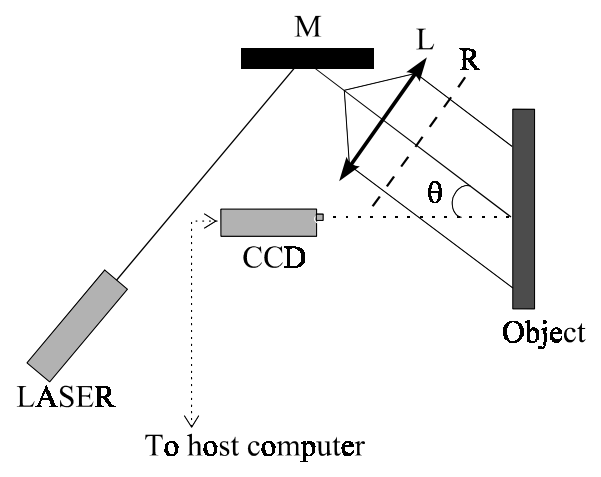


Figure 1 Experimental setup. M: mirror, L: lens, R: Ronchi granting, θ : angle of incidence.

A first image of the object thus illuminated is acquired and stored in the memory of a frame grabber. After a tilt of the object, the reference frame stored in memory is continuously subtracted from the incoming actual image, and then the intensity difference is displayed. This operation gives rise to a moiré pattern in the TV monitor without the need of another grating. We can consider the situation as equivalent to the case of superposition with a virtual grating corresponding to the first stored reference image. The contrast of these moiré fringes can be as high as 100%. As expected, the moiré fringes are oriented parallel to the rotation axis of the object, regardless of the direction the fringes in the grating may form with respect to that axis.

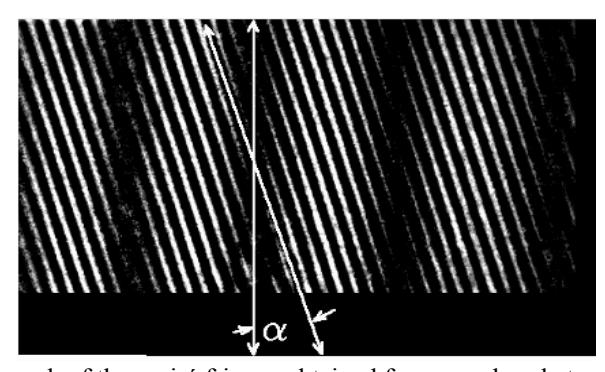


Figure 2 Photograph of the moiré fringes obtained for an angle α between the direction of the grating and the rotation axis.

Figure 2 is an example of this situation. As we intend to reduce the time of fringe interpretation and to implement the automatization of the measurements, we first obtain a transfer curve under controlled laboratory conditions. According to this idea, the test object is mounted on a precision rotational stage, then we get a curve representing the spacing of the moiré fringes versus the rotation angle, as shown in Figure 3.

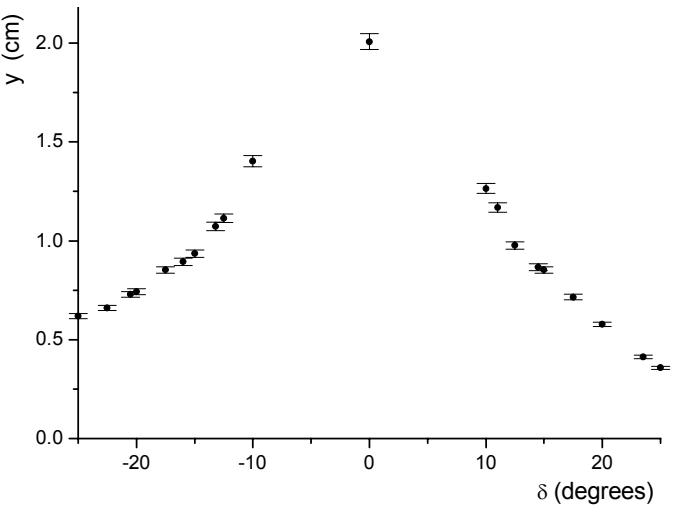


Figure 3. Example of transfer curve: moiré fringe separation as function of the rotation angle δ .

The geometrical parameters associated with the moiré pattern are: the angle of incidence of the illuminating beam (θ) , the period of the grating at the object (i.e. which Talbot replica is used), the angle (α) between the Ronchi ruling direction and the rotation axis of the object, and the magnification of the optical imaging system of the camera lens. We assume the parallelism between the observation and the recording axis. By using the transfer curve under the above conditions, we only need to know the angle (α) . Measuring the fringe spacing, and multiplying this value by $\cos\alpha$ we obtain from the transfer curve the rotation angle. The noticeable asymmetry in the curve with respect to the origin is due to the angle subtended between the Ronchi grating and the camera. The smaller this angle, the more symmetric the curve. It is interesting to know the

factors limiting the sensitivity of the method. Quality of the image is important in the sense of having a well-defined fringe system. Unlike the case of digital interference fringes, the contrast of these moiré fringes is almost unity. From Figure 2, we can distinguish, besides the moiré system, those carrier fringes of the Ronchi ruling. Precisely, from this feature we can measure the angle α , as moiré fringes are parallel to the rotation axis.

The problem of fringe spacing measurement can be overcome by FFT methods, which allow frequency measurements with high accuracy. The requirement of at least three moiré fringes sets a lower limit to the minimum tilt to be detected. From the plot of Figure 4, we show the fringe spacing times $\cos\alpha$ versus α , for a 15° tilt of the object. No appreciable error is introduced in the measurements of the tilt. Once the transfer curve is obtained for a given optical configuration, the procedure can be applied in other environments outside the laboratory. The recording can be done even with the help of a camcorder to process the results in a second step in the laboratory. A wide range of objects can be inspected but it is mainly devoted to control large mechanical objects whose relief is preferably monotonic. With respect to the parallelism in the projection-observation axis, we can tolerate a certain inaccuracy as a small error in this positioning has little influence on the fringe analysis.

Another important problem to overcome is the sign of the tilt, which has to be determined before using the transfer curve. This can be accomplished by introducing fiducial markers observed through the CCD camera, or by introducing a 'reference' tilt of known sign and tracking the fringes to see whether the spacing increases or not, indicating that the actual tilt sign is opposite or not to the reference tilt respectively.

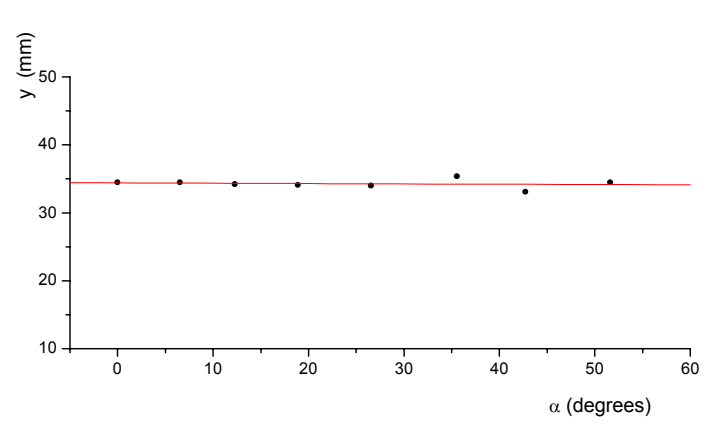


Figure 4 Representation of the moiré fringe spacing multiplied by $cos(\alpha)$ for a 15° tilt of the object.

This fringe tracking also allows to locate the rotation axis as, if it falls on the camera field of view it is represented by a motionless fringe, and if it lies outside this view region, the fringes move towards the side on which this axis is located.

A mislocation of the Talbot image as well as a large tilt may introduce a loss in fringe visibility. Strictly speaking, the Talbot effect is a diffraction phenomenon and consequently we cannot relate to it a depth-of-field. However, it is clear that aperture diffraction diminishes the contrast above a certain Talbot plane. Although we can associate a transfer function to this wave propagation effect, there is only one plane for every Talbot image to be well defined. In the neighborhood of this plane a shadow of the Talbot image is seen, with a progressive loss of sharpening as we move farther apart. To investigate the possible visibility misinterpretation due to the existence of the nearest so-called fractional Talbot plane, we calculate the position of such plane as $\Delta = (Z_{n+1} - Z_n)/4$, measured from the object plane. For example, a 50 l/inch grating has a Δ = 51.2 mm. As there is no need to record a large portion of the object to obtain the moiré pattern, we see that the maximum departure from the Talbot plane for a 2 cm imaged portion of an object tilted 15° around an axis centered on it is 2.7 mm. This departure is well under the distance to introduce a confusion between Talbot planes and lies within a range in which the Talbot images still have an acceptable visibility to produce detectable moiré fringes. In practice, fringe patterns with such low visibilities as 0.1 can be readily detected with Fourier transform methods

[7], even if they are immersed in speckle noise. We experimentally verified that such moiré patterns are produced for displacements of around 40% of Δ . As Δ can be increased by decreasing the grating frequency, the problem of a large departure from the Talbot plane due to the object rotation can be partially overcome. For instance, with our earlier example it means a 2 cm departure, which in turn for the same 15° tilt occurs at 7.5 cm away from the rotation axis. For a 12.5 l/inch ruling this last distance is 118 cm. Accordingly, it must be kept in mind that this distance decreases dramatically for a 100 l/inch ruling or a greater frequency.

To establish the accuracy of the method we make the following analysis. If α represents the angle between the rotation axis and the Ronchi ruling direction, δ is the object tilt angle, P_m the pitch of the moiré fringes, P_1 is the pitch of the Talbot image on the object and P_2 the pitch of P_1 projected on the new tilted plane, then [8]

$$1/p_{\rm m}\cos\alpha = 1/p_2 - 1/p_1 \tag{1}$$

or, as $p_2 = p_1 \cos \delta$

$$1/p_{\rm m} = 1/p_1[(1/\cos\delta - 1)]\cos\alpha$$
 (2)

Since this method is based on fringe spacing changes, a simple and practical accuracy limit depends on the minimum resolvable fraction of a fringe introduced by the tilt.

The number of fringes N on an image is a/p, where a is the size of the imaged portion, then

$$N_{\rm m} = N[(1/\cos\delta) - 1]\cos\alpha \tag{3}$$

with N_m the number of fringes on the moiré pattern and N_t the number of fringes on the imaged object Talbot plane. The fraction of a fringe ΔN_m introduced by a variation of the rotation angle $\Delta \delta$ is

$$\Delta N_{\rm m}/\Delta \delta = |N_{\rm t} (\sin \delta/\cos^2 \delta) \cos \alpha| \tag{4}$$

As an example to illustrate the approach, let us consider the case of a 50 l/inch Ronchi ruling with one of its self-images on a 8 cm wide image area object under He-Ne laser light illumination ($\lambda=0.6328~\mu m$). We have $N_t=160$ fringes, and according to Eq. (3) $N_m=5.64$ fringes. If $\alpha=0$ and the object tilt is of around $\delta=15^\circ$, then $\Delta Nm/\Delta\delta=0.77$ fringe/degree, that is a $\Delta\delta=0.1^\circ$ (≈ 0.001 rad) introduces a $\Delta Nm\approx0.08$. As we have 5.64 dark fringes, then there are approximately 45.5 pixels/fringe. Besides, we are able to detect a change in fringe spacing of 2 pixels. In our case this means $\Delta Nm\approx0.04$, denoting we can resolve such $\Delta\delta$. The method exactitude is just sufficient for the control of large mechanical objects, but the accuracy is not maintained if the rotation angle becomes large ($\delta > 45^\circ$)

2.<u>OBJECT POSITIONING BY A DIGITAL MOIRÉ FOCUSING</u> TECHNIQUE

Object positioning techniques are important methods related to machine vision and imaging. The performances of existing techniques depend mainly on sharpness of fringes, noise sensitivity and processing time. They generally employ gray level variance [9,10], image visibility [11], Laplacian [12,13] and fringe contrast [14] to name a few.

In this work we present an alternative method based on digital Moiré fringe contrast measurements as a focus measure to object positioning.

The principle of the method relays on the fringes visibility mismatch [15] in the Moiré process while defocusing occurs due to object mispositioning, which induce a lost of fringe contrast. A theoretical model of this mismatch is also given. Based on this model we prove our assumption of measuring a global maximum for the best focused grating image, and consequently the best contrast in the moiré fringes. We investigate several alternatives, both under laser light and white light illumination, as well as the advantages of introducing the possibility of use the Talbot or self-imaging effect.

We analyze the signal-to-noise ratio from the statistical point of view, which contains the focusing information. Our approach is very simple to implement, reliable and allows an accuracy of 0.5 mm, which is sufficient for a wide range of industrial and technical applications.

2.1.THEORETICAL MODEL

The basic optical scheme is depicted in Figure 5. Light from a He-Ne laser source illuminates a Ronchi ruling R. A self-image of R is formed in the plane Π . The object is mounted on a precision translation stage which can be moved along the z axis. A CCD camera sees the object through a beam splitter BS.

If instead of a laser, an incoherent source is used, an imaging lens has to be added to project an image of R on the plane Π .

We assume first that the best focused position is not in the image plane, consequently a blurred or defocused grating image is formed at plane P. In our case the target object is moving along and it is to be positioned at a previously established plane.

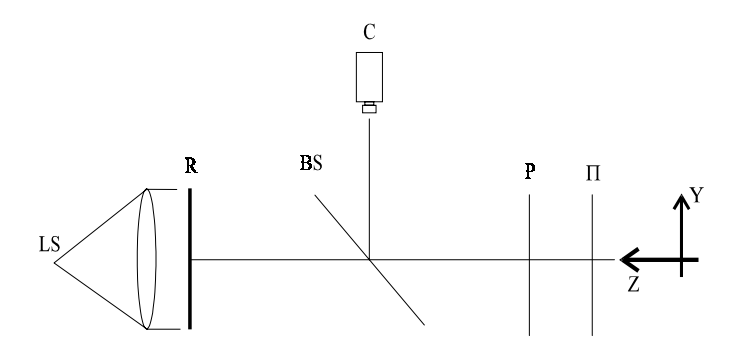


Figure 5 Experimental set-up for the case of laser illumination and self-imaging effect. When using incoherent light a focusing lens has to be added. LS is the light source , R is a Ronchi ruling, BS a beam splitter and C is a CCD camera. Π is the focusing plane. P is the plane where the reference image is taken .The object is moved along the z axis on a precision translation stage.

We can define a fringe intensity function in the form

$$f_k(m,n) = |I(m,n) - I'_k(m,n)|$$
 (5)

where I is the intensity function for the moiré fringes at the best-focused plane of the reference grating, and I_k ' is the moiré intensity function corresponding to the reference grating rotated an angle θ and taken at a defocused plane k along the z-axis.

Care must be taken in choosing the right angle θ , as if the angle is too high the Moiré fringes visibility itself decreases.

The matching function for f_k is defined as

$$MF_{k}(m) = \frac{1}{MxN} \left\{ \sum_{n=1}^{M} \sum_{j=1}^{N} \left[f_{f}(m,n) - f_{k}(m,n-j) \right]^{2} \right\}^{\frac{1}{2}}$$
 (6)

This function thus describes the Moiré fringes profile as an average taken over a window of MxN pixels, along a sampling line m arbitrarily taken as the center of the window.

In our procedure, we take the maxima and minima of every $MF_k(m)$, so that we can define

$$I_{k \text{ max}} = \frac{1}{T} \frac{1}{R} \sum_{i=1}^{T} \sum_{m=1}^{R} [MF_{k}(m)]_{i_{max}}$$
 (7)

and

$$I_{k \min} = \frac{1}{T'} \frac{1}{R} \sum_{i=1}^{T'} \sum_{m=1}^{R} [MF_k(m)]_{i_{\min}}$$
 (8)

with T, T' the number of maxima and minima respectively within each window, while R represents the number of different positions the sampling window may take within the whole image.

Accordingly, the visibility for every k-plane can be found as [16]

$$Fv_k = \frac{I_{k \max} - I_{k \min}}{I_{k \max} + I_{k \min}}$$
 (9)

For the intensity extrema measurements the standard deviation is expressed as

$$\sigma = \left\{ \frac{\sum_{m=1}^{R} [MF_k(m) - I]^2}{R - 1} \right\}^{\frac{1}{2}}$$
(10)

where I is defined either by eqs. (8) or (9). If σ_1 is the standard deviation for a one pixel measurement (M=1, N=1), then

$$\sigma = \frac{\sigma_1}{(MxN)^{1/2}} \tag{11}$$

This procedure strongly reduces the noise effect produced by single pixel detection immersed in speckle or by the white light background. Furthermore, there is no need for applying average filters or FFT algorithms. Besides, the direct image, without preprocessing, can be used, thus reducing the computing time. The operation is highly effective even in the case of low visibility fringes, eliminating also the use of sharpening filters.

2.2 EXPERIMENTAL RESULTS

Back to Figure 5, we positioned our test object where an image of a ruling was formed. The test object was also mounted on a precision translation stage. Experiments were conducted in planar test objects. An image of the ruling was then taken with the CCD camera and stored in the memory buffer of the frame grabber. This image will serve as the reference for obtaining the moiré fringe pattern. The grating is rotated around its own plane and the digital subtraction operation is performed and the result stored. As a result, a set of moiré fringes appear on the TV monitor. The procedure is repeated for several other positions of the object, but always having the same reference image of the

buffer for the subtraction and not altering the focusing of the CCD camera. For every stored image we applied the method described in the above section to obtain a curve showing the visibility of the moiré fringes as a function of the displacement with respect to the first stored reference

position. We applied our proposal both using laser light and white light illumination. In the first case we employed amplitude and phase gratings, but also in both cases using the Talbot effect to produce the image of the grating on the desired plane. This plane can be exactly positioned by using the Talbot expression $Z_T = 2nd2/\lambda$, with d the period of the grating and n an integer, while Z_T is measured from the true grating plane. With an appropriate choice of the period, the plane to be focused can be adequately positioned. Consequently, there is no need for any imaging forming system for the grating. Light diffraction sets also a limit to the useful Talbot image plane, as they loose contrast when moving too far from the actual grating. Figure 6 shows a plot for a 2 l/mm frequency grating to compare both an amplitude version and a phase grating version. Phase grating shows a better performance, as allows more light to pass and contains less speckle noise.

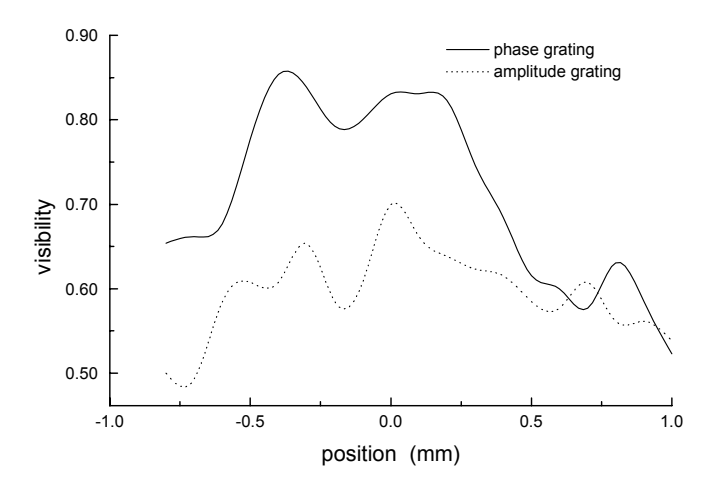


Figure 6 Visibility curves for amplitude and phase 2 l/mm rulings for a given Talbot plane.

However, in both cases the best-focused plane is readily detected from the plot, as it has always the maximum Moiré fringe visibility. The other secondary peaks belong to the so called fractional Talbot planes ever present in this phenomenon. They are replicas of the ruling, but with an appreciable lower contrast, as confirmed also from the experimental data.

The white light version of the Talbot effect, called Lau effect, offers no advantages as an intrinsic blurring of the grating self-images due to the various wavelengths involved. For this reason, under white light illumination we use an imaging forming system to bring the grating image to the desired focusing plane. In this circumstance phase gratings are not employed.

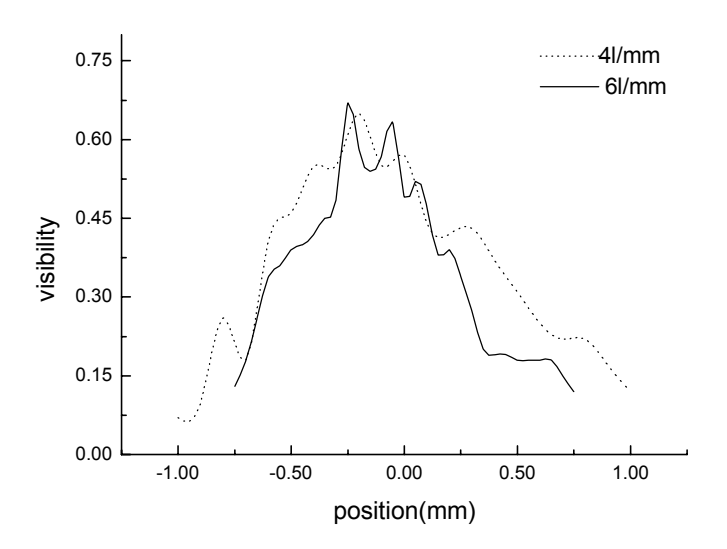


Figure 7 Comparison between 4 l/mm and 6 l/mm rulings, for a case in which the reference grating image is not in focus.

Figure 7 is an example for gratings of different periods, which also illustrates the case where the camera is slightly defocused. Even in this situation, the object can be adequately positioned, as the maximum visibility is always attainable at the plane where the grating image is formed.

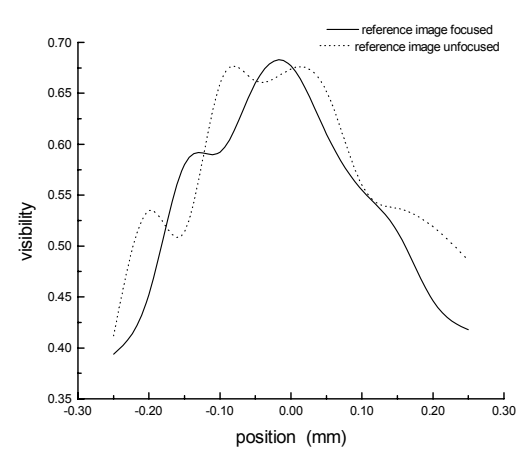


Figure 8 Visibility curves for a 4 l/mm grating showing the case of focused and defocused reference image .

For Figure 8 the defocusing was corrected, and the only appreciable effect is a small contrast enhancement.

In all plots, positive distances are defined to the light source position, and the opposite for the negative values. This explain the fact that the curves are not symmetrical with respect to the best-focused plane, as there is more background light to the source side than to the other.

It has to be stressed that the main advantage over direct fringes visibility measurements on projected fringes is the higher visibility decay shown in Lau fringes. To illustrate this point we present the plot in Figure 9, where the theoretical curves of the visibility for both cases are represented as a function of the z translation along the optical axis. In the case of the projected fringes the curve obeys to the formulation [17] $\sin c^2(\alpha)$ with $\alpha = \pi a^2 z/2\lambda f^2$, being a/f the numerical aperture of the grating imaging system. For the Lau effect the visibility is described by the formulation proportional to $\cos(\alpha)$ [18], where $\alpha = \pi \lambda z/p^2$ and p is the pitch of the grating. In these cases we assumed the first Lau image as reference for the plot. For this visibility comparison to be valid we adopted the situation in which $p = \lambda f/a$, otherwise it is not possible to establish a relationship. It is clearly seen that the z value for zero visibility coincides with the well-known zero-contrast Lau image position.

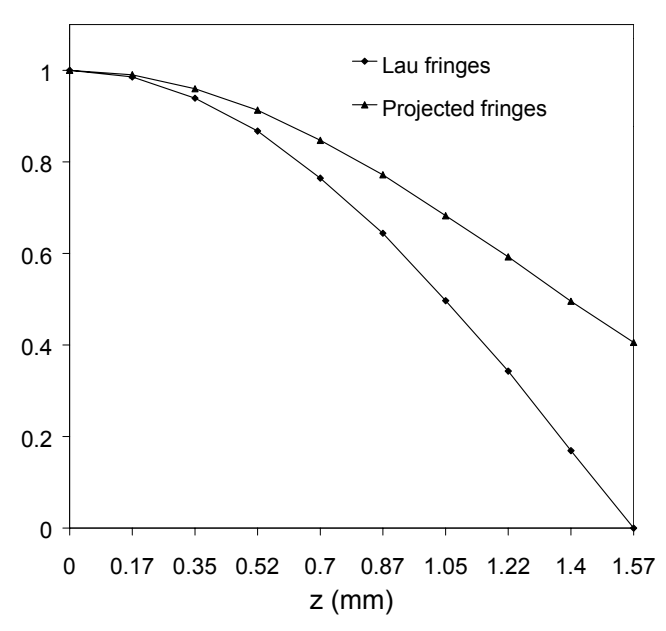


Figure 9 Theoretical visibility curves for both projected and Lau fringes, as function of object displacement z. Lau fringes contrast diminish faster for the same displacement

2.3 <u>DISCUSSIONS ON THE METHOD</u>

It is important to mention the limitations of the method: as we take image intensity differences to obtain the digital Moiré pattern, an intrinsically low intensity range is achieved. In this sense, extremely low intensity values are handled such that also in several cases I_k max $\approx I_k$ min , so care must be taken in using eq. (9) as in that instance it may be no longer valid. Sensitivity can be increased by using gratings with a higher spatial frequency, but at the expenses of an initially lower Moiré fringe visibility, as the higher the frequency the less transmit the light the amplitude gratings.

The reflectivity of the object to be focused also influences the Moiré visibility, but light intensity from the illuminating source can be so adjusted as to compensate this problem.

A typical video camera has a resolution in terms of fringes of about 27 l/mm, then the detector resolution imposes no limitation on the spatial frequency for most commercially available Ronchi rulings.

The accuracy range depends on the grating period, but for most practical uses with a frequency extent between 1 to 12 l/mm, the object can be positioned with a precision less than 0.5 mm. Moreover, with a few steps the best focused plane can be found.

White light illumination probed to be more convenient as quality of the results are comparable to those with laser light, with the additional advantage of high intensity availability, easy adjusting and adaptation to work in hostile environments. As a disadvantage, a lens system has to be used to image the grating thus introducing a source of error. In the case of laser light such disadvantage does not exist as the image is located trough the Talbot effect thus diminishing that error. Further experiments demonstrated that a slight higher accuracy is attainable with coherent light, but at the expenses of a growth in speckle noise and a consequent increase in processing time.

While measuring the sensitivity to detect visibility changes as a function of the grating pitch, we observed that in the range of the spatial frequencies studied, there are not appreciable variations.

A compromise has to be made between the window wide and the fringe contrast, because for small contrast fringes, a large window can lead to an average which gives an almost constant matching function.

<u>REFERENCES.</u>

- [1] Teokaris, P., Viafiadakis, A., Liakopoulos, C.: "Theory of spatial moiré fringes",1968. J. Opt. Soc. Am. 58, 1092-1099.
- [2] Teokaris, P. 1962. Strain Analysis, Pergamon Press, first edition.
- [3] Der Hovanesian, J. & Hung, Y.Y.: "Moiré contour-sum, contour-difference, and vibration analysis of arbitrary objects", 1971. Appl. Optics 10, 27342738.
- [4] Takasaki, H.: "Moiré topography", 1970. Appl. Optics 9, 1467"1472.
- [5] Idesawa, M. Yatagai, T., Soma, T.: "Scanning moiré method and automatic measurement of 3-D shapes", 1977. Appl. Optics 16, 2152-2162.
- [6] Lohmann, A.W. & Silva, D.A.: "An interferometer based on the Talbot effect", 1971. Opt. Comm. 2, 413-415.
- [7] Pomarico, J. & Torroba, R.: "Digital visibility measurements by Fourier analysis", 1994. Optik 95, 152-154.

- [8] Patorkski, K. 1989. In: Wolf. E. (Editor), Progress in Optics XXVII, Page 3-108, North Holland, Amsterdam.
- [9] Subbarao, M., Choi, T., Nikzad, A.:"Focusing techniques", 1993 Optical Eng. 32, 2824-2836.
- [10] Lee, J.H., Kim, K.S., Nam, B. D., Lee, J. C., Kwon, Y.M., Kim, H.G.: "Implementation of a passive automatic focusing algorithm for a digital still camera", 1995. IEEE Trans. Consumer Electron. 41, 449-454.
- [11] Torroba, P., Cap, N., Rabal, H.: "Defocus correction using a visibility criterion", 1994. J. Modern Optics 41, 111-117.
- [12] Lightart, G & Groen, F.: "A comparison of different autofocus algorithms", 1982. In: Freitag, H. (Editor), proceedings of IEEE International Conference on Pattern Recognition, Page 597-600, IEEE New York.
- [13] Krotkov, E.: "Focusing", 1987. Int. J. Comput. Vision 1, 223-237.
- [14] Akiyama, N., Makihira, H., Nakata, T.: "Automatic focusing method using stripe patterns projection technique II: subjects and countermeasures for practical use", 1990. J. Jpn. Soc. Precis. Eng. 56, 2273-2279.
- [15] Bryanston-Cross, P. & Wang, Z.: "Camera focusing based on fringe pattern matching", 1997. Appl. Optics 36, 6498-6502.
- [16] Lehman, M., Pomarico, J., Torroba, R.: "Digital speckle pattern interferometry applied to a surface roughness study", 1995. Optical Eng. 34, 1148-1152.
- [17] Born, M. & Wolf, E. 1983. Principles of Optics, Pergamon Press, Page 435-442, sixth edition.
- [18] Jinhong, T.: "The diffraction near fields and the Lau effect of a square-wave modulated phase grating", 1988. J. Modern Optics 35, 1399-1408.